Journal of Machine Engineering, 2019, Vol. 19, No. 2, 83–98
ISSN 1895-7595 (Print) ISSN 2391-8071 (Online)

Received: *28 January 2019* / Accepted: *12 April 2019* / Published online: *29 June 2019*

paddle forming, paddle shape optimization,
incremental hole-flanging,
strain path mapping

Lemopi Isidore BESONG[1*]
Johannes BUHL[1]
Markus BAMBACH[1]

PADDLE SHAPE OPTIMIZATION FOR HOLE-FLANGING BY PADDLE FORMING THROUGH THE USE OF A PREDEFINED STRAIN PATH IN FINITE ELEMENT ANALYSIS

This research investigates a novel hole-flanging process by paddle forming through the use of finite element (FE) simulations. Paddles of different shapes rotating at high speeds were used to deform clamped sheets with pre-drilled holes at their centers. The results of the simulations show that the paddle shape determines the geometry and principal strains of the formed flanges. A convex-shaped paddle forms flanges with predominant strains in the left quadrant of the forming limit diagram (FLD). However, the convex paddle promotes unwanted bulge formation at the clamped end of the flange. A concave paddle forms flanges with no bulge but the principal strains of elements in the middle section of the flange are in the right quadrant of the FLD which indicates an increased probability for crack occurrence. An optimization of the paddle shape was conducted to prevent bulging at the clamped end while avoiding crack occurrence. The paddle shape was optimized by mapping the deformation of some elements along the flange length to a pre-defined strain path on the FLD while maintaining the bulge height within the desired geometric tolerance. The radii and lengths of the paddle edge were varied to obtain an optimum paddle shape.

1. INTRODUCTION

Hole-flanging is the process of expanding holes in sheet metals to form flanges. In conventional hole-flanging, the blank is held in place at its edges by clamps while the flange is formed by the displacement of dies and punches. The geometries of the dies and punches are maintained within close tolerances to obtain the desired deformation of the blank. This reduces the flexibility of the process. New die sets are required to produce parts with different shapes. Forming dies are expensive and greatly increase process set up costs [1]. This makes conventional hole-flanging economically viable only for large batch production where the high cost of die sets can be spread between a large number of products.

[1] Chair of Mechanical Design and Manufacturing, Brandenburg University of Technology Cottbus-Senftenberg, Cottbus, Germany
* E-mail: besonlem@b-tu.de
https://doi.org/10.5604/01.3001.0013.2226

Highly competitive present-day markets cause manufacturing enterprises to reduce the size of batches of production in order to satisfy a wide range of demands so as to maintain or increase their market share and thus maximize profit [2]. This entails a change from high volume production to smaller batch sizes with more product variants. Incremental sheet forming (ISF) processes can serve as an alternative to conventional forming for small batch production and prototype manufacture due to their low cost and high flexibility [3]. These processes also provide high formability compared to conventional forming [4]. Hole-flanging by single point ISF using a multi-stage tool path strategy was developed by Cui and Gao [5]. The process has setbacks such as a long process time and poor geometrical accuracy [6]. Allwood and Shoulder proposed ISF by paddle forming as alternatives for conventional forming processes to benefit from their dieless nature, low set up cost and increased formability [7].

This study uses FE analyses to investigate the feasibility of applying a paddle forming procedure to hole-flanging. The hole-flanges are made by forming clamped sheets with pre-drilled holes using paddle-shaped tools rotating at high speeds while being displaced at high axial feeds. The blanks are deformed incrementally from the edge of the holes to the clamped ends. The simulation results reveal a need to optimize the paddle shape in order to prevent cracks and bulge formation. The setup of the hole-flanging process based on paddle forming is shown in Fig. 1.

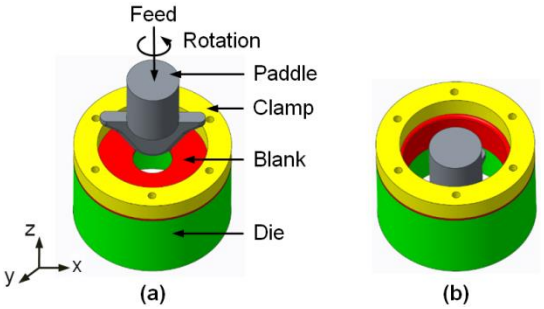

Fig. 1. Setup of the hole flanging process by paddle forming. (a) Start of the process. (b) End of the process

2. DETERMINING THE EFFECT OF THE PADDLE SHAPE ON THE HOLE-FLANGING PROCESS THROUGH THE USE OF FE ANALYSES

The results of numerical simulations present good insights into certain aspects of manufacturing processes such as forming limits and process mechanics during forming. This leads to a significant reduction in product development time and costs required to conduct experiments. FE simulations were conducted to study the effect of paddle shape on the geometrical accuracy and principal strains in the flanges. Ideally, the principal strains of the formed flanges should be in the left quadrant (safe zone) of the FLD and the deformation of the flange should follow a pure shear (constant thickness) strain path. For the pure shear strain path β, $-\varphi_2/\varphi_1 = -1$; where φ_2 = minor true strain, φ_1= major true strain. This strain path avoids splitting of the flange and the occurrence of biaxial stretching

which promotes crack development [8]. This leads to flanges with large hole expansion ratios. In addition, poor geometrical accuracy is a major setback to the use of ISF processes. A geometrical tolerance of ±0.2 mm is required over the entire surface of the flanges in order to meet industry standards [9]. The flanges from the simulations should meet these 2 criteria before proceeding to physical experiments on the process.

2.1. FINITE ELEMENT ANALYSIS

FE simulations were carried out on aluminum alloy EN AW-6181-T1 sheets of 0.8 mm thickness. The mechanical properties were determined from tensile tests carried out on a tensile testing machine (Zwick 250), based on DIN EN 10002-1 tensile test standards. The mechanical properties are obtained as follows; yield strength R_{eH} = 165 MPa, maximum tensile strength R_m = 360 Mpa, elastic modulus E = 65 GPa, percentage elongation at fracture A_g = 24%, hardening exponent n = 0.23 and strength coefficient k = 510 MPa.

The aluminum sheets were defined as deformable shells with an isotropic elastoplastic material behavior and a hardening law as derived from the tensile tests. The paddles, clamp, and die were considered as non-deformable rigid bodies. A coefficient of friction of 0.1 was assigned to the contact surfaces. The clamp and die had inner diameters of 50 mm and 40 mm, respectively. Blanks with a hole diameter of 13.3 mm were used to form flanges with the paddles rotating at a speed of 1000 rev/min and an axial feed of 1500 mm/min. The effects of temperature on the process were neglected in the simulations. An implicit dynamic solution scheme was employed in LS-DYNA. Implicit analyses were used because they have been shown to produce parts having geometries close to the shapes of products obtained by ISF experiments, since the spring back of the blank is calculated for every timestep [10].

2.2. PADDLE DESIGN

To determine the effects of the paddle shape on the hole-flanging process, FE simulations of the process were conducted using convex and concave paddles. These paddle shapes were chosen from many possibilities because they yield different strain distributions. Both paddles had a 40 mm diameter and were designed to make a line contact with the blank. The convex and concave paddles are shown in Fig. 2.

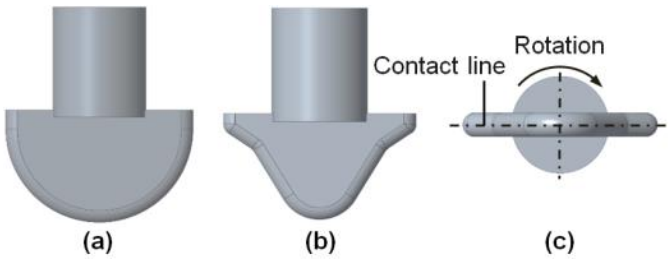

Fig. 2. a) Front view of the convex paddle. b) Front view of the concave paddle. c) Bottom view of the concave paddle

2.3. GEOMETRICAL ACCURACY

Geometrical accuracy measurements of the flanges obtained from the numerical simulations reveal a significant difference in bulge heights at the clamped end (see Fig. 3) of the flanges due to a change in paddle shape. The bulge heights at the clamped end of the flanges were 2.23 mm for the convex paddle (this value is 11 times worse than industry standards for geometrical accuracy [9]) and 0.01 mm for the flange formed by the concave paddle. The change in the bulge height is a result of the small radius at the edge of the concave paddle pulling the material into the die during the process which prevents bulge formation. The shape of the convex paddle allows upward movement of the sheet from the bottom of the die towards the top due to the stiffness of the sheet resisting deformation. This causes the high bulge at the clamped edge of the flanges formed by the convex paddle, Fig. 3a.

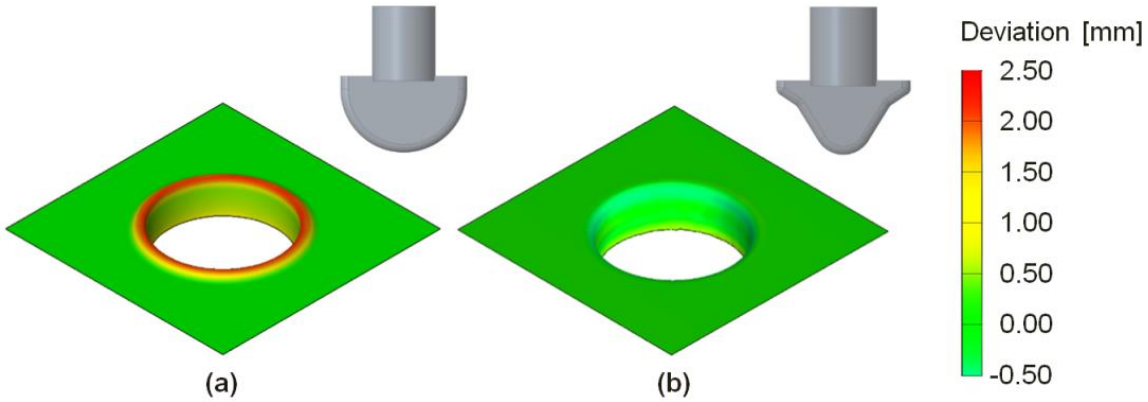

Fig. 3. a) Flange formed using the convex paddle. b) Flange formed using the concave paddle

2.4. STRAIN EVOLUTION

The evolution of the principal strains in the FLD is studied for 3 points along the length of the flanges made by the 2 paddles to understand the effect of the paddle shape on the process mechanics, see Fig. 4a and 4b. At the edges of the flanges (point A), the strain paths are similar for both paddle shapes. The elements in this region undergo maximum deformation and experience uniaxial tension. At point B, mid-way along the flange length, the strain path moves towards biaxial tension for the concave paddle as shown in Fig. 4b. An explanation for the biaxial tension at point B is the concave paddle has a small radius at its edge which leads to stress localization. Biaxial tension indicates that the sheet is thinning and heading towards fracture. The convex paddle has a large radius which prevents biaxial tension; thus the strain path remains in uniaxial tension for the convex paddle. The strains at point C are small in magnitude. For the flange formed by the concave paddle; the element at C is in uniaxial tension due to the paddle drawing the blank into the die, see Fig. 4b. The strains are in the wrinkling zone for the convex paddle, as presented in Fig. 4a. This is supported by the high bulge observed for the flange made with the convex paddle in Fig. 3a.

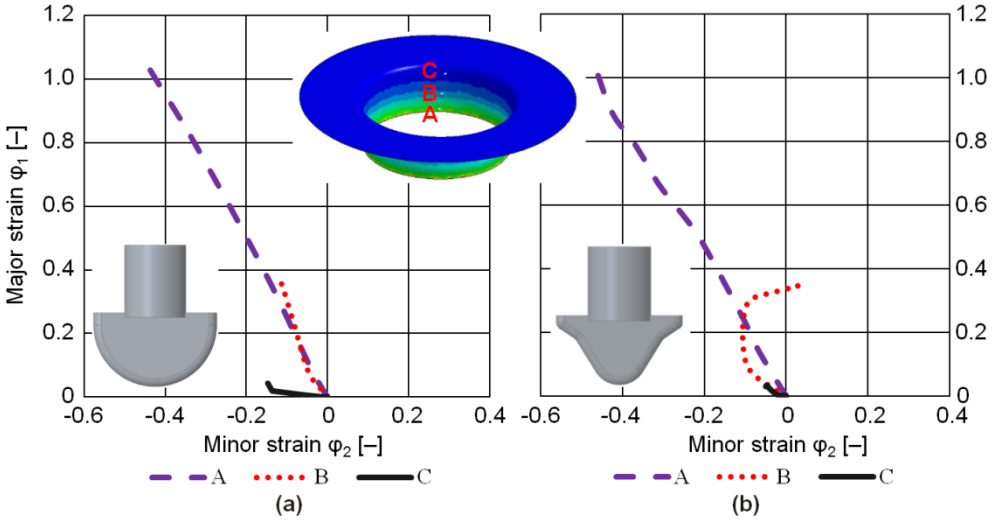

Fig. 4. Evolution of the major and minor strains at 3 points: a) convex paddle, b) concave paddle

3. PADDLE SHAPE OPTIMIZATION

The results of the FE simulations reveal a need to optimize the paddle shape to obtain a paddle which forms flanges in the safe region of the FLD at point B while maintaining low bulge heights at the clamped end of the flange. To achieve these two objectives, an optimization of the paddle shape was carried out by FE simulations using the LS-OPT software.

3.1. DESIGN OF OPTIMIZATION PARAMETERS

The optimization was carried out with the aid of a curve mapping strategy in LS-OPT. The paddle shape was altered to achieve deformation of the flange following the desired curve (strain path) while keeping a low bulge height. The bulge is formed in the 5 mm length of the blank left unclamped between the inner diameters of the die and clamp. The nodes used to obtain the bulge heights from the FE simulations are shown in Fig. 5a. A geometric tolerance $h = \pm 0.2$ mm was prescribed as the maximum allowable deviation of the bulge height.

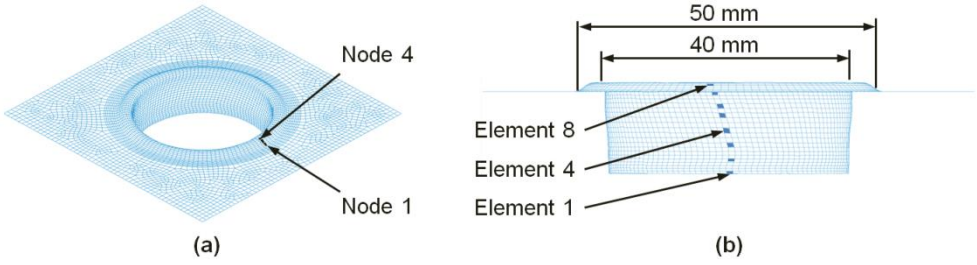

Fig. 5. a) Nodes used to obtain bulge height, b) Elements used to extract strain along the flange length

The principal strains were obtained for 8 elements along the length of the flange from the simulations, see Fig. 5b. The strains were mapped to a pre-defined strain path on the FLD. The optimization procedure aims at reducing the distance (D) between the desired (target) strain path and the strains from FE simulations. This is done by adjusting the design variables so that the principal strains from the FE simulation move towards the target strain path. The derivation of D can be found in [11], see appendix. Figure 6a shows the definition of the objective function using the curve mapping strategy. Optimization by curve mapping strategies has been carried out in [12, 13].

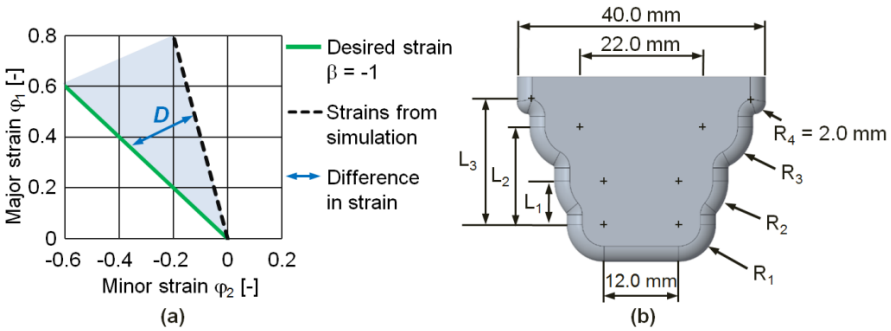

Fig. 6. a) Definition of strain path for optimization, b) Paddle shape parameters

The paddle shape was designed to mimic multistage single point ISF with a single tool. The 4 radii along the edge of the paddle represent 4 forming stages, see Fig. 6b. The variables altered during the optimization process include the radii of 3 forming edges (R_1, R_2, and R_3) and the lengths of 3 forming edges (L_1, L_2, and L_3), as shown in Fig. 6b. R_2 was made a dependent of R_1 ($R_2 = R_1 + 2$) to reduce the number of variables in the optimization. The radius of the 4th forming edge (R_4) was not varied in order to maintain the paddle diameter at 40 mm. However, its length (L_3) was varied. The base of the paddle was kept constant at a diameter of 12.0 mm. A drill bit is attached to this end of the optimized paddle during the experiments.

3.2. OBJECTIVE FUNCTION AND CONSTRAINTS

A series of test FE simulations were conducted to determine the boundaries of the variables to be used in the optimization. From the simulation results, it was found out that a small radius is needed at the final forming edge to maintain low bulge heights. Thus, the radius of the last forming edge (R_4) was kept constant at 2 mm. An optimization was carried out using the full range of the paddle edge radii R_1, R_2, and R_3. The optimum paddle shape obtained from the optimization formed the flange using only 2 edges of the paddle. To ensure that all the 4 edges of the paddle form the flange, the boundaries of the variables were reduced, see table 1. The optimization problem can be formulated as a minimization of the distance D, subject to the boundaries of the variables and geometrical accuracy presented in Table 1. The starting values of the variables for the optimization are presented in Table 1 (L_1, L_2, L_3 – length from the center of the first edge, R_1, R_2, R_3 – radius of edges, h – deviation from the target geometry).

Table 1. Table of variables

Variables	Lower boundary (mm)	Upper boundary (mm)	Starting value (mm)
L_1	3	10	3
L_2	7	20	7
L_3	5	20	10
R_1	3	6	3
R_2	5	8	5
R_3	5	8	8
h_i	-0.2	0.2	

A paddle shape obtained by parametrization is shown in Fig 7a. Fig 7b presents the set up used in the FE simulations.

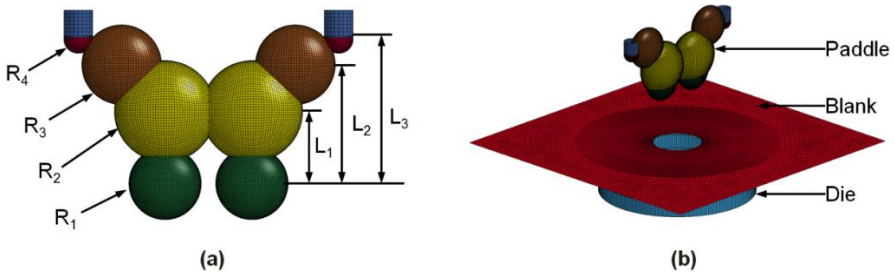

Fig. 7. a) Tool shape parameters b) Finite element analyses set up

3.3. OPTIMIZATION SET UP

FE simulations were conducted at various levels of the variables (radii and lengths of the paddle edges) with the aim of optimizing the responses (principal strains and bulge height). The set-up of the optimization is as follows:

Step 1: Start of the optimization process. At the start of the optimization process, a link was made between the optimizer (LS OPT) and the FE setup (LS PREPOST). The geometry of the paddle was varied through parameterization of the paddle shape in LS PREPOST by use of a command file script.

Step 2: Set up of FE analyses and optimization model. The FE simulations were built with a constant paddle speed and feed, mesh size of the blank, coefficient of friction and clamping condition. The desired responses from the simulations, optimization procedure, curve mapping strategy and boundaries of the variables were defined in LS OPT.

Step 3: Design of experiments (DOE). The optimization model uses a DOE based on D-optimal point selection scheme with a linear approximation. This point selection method requires fewer experiments than a full factorial design for problems with many design variables [14]. 12 FE analyses were conducted per iteration.

Step 4: Meta model. The responses from the FE analyses were used to construct meta models. Response surfaces (RS) were obtained from the meta models which describe the behaviors of the parameters for each iteration.

Step 5: Multi-objective genetic algorithm (MOGA). Genetic algorithm (GA) was used to determine the optimum from the meta models. GA is better at determining the optimum

solution for large optimization problems compared to traditional (gradient based) optimization methods which usually get stuck in local optima. The default setting of GA in LS OPT was used for the optimization since it has been shown to be efficient at determining the optimum solution for most optimization problems [14]. MOGA was used in this study because it reflects a trade-off of the solutions of the individual elements.

Step 6: Termination criteria. The accuracy of the optimization was defined using specified tolerances for design change and objective function change. The MOGA terminated when these tolerances were met.

Step 7: Sequential response surface methodology (SRSM). SRSM was carried out with domain reduction to reduce the size of the region of interest (design space) and refine the results of the optimization after each iteration. SRSM is done by moving and/or reducing the region of interest around the optimum with a prescribed tolerance zone around it.

Step 8: Update design variables. New variables were determined for the updated design space after domain reduction. The cycle restarts from step 2 and is repeated for 8 iterations. An FE analysis was carried out for the optimal design to verify the optimum solution. The optimization procedure is shown in Fig. 8.

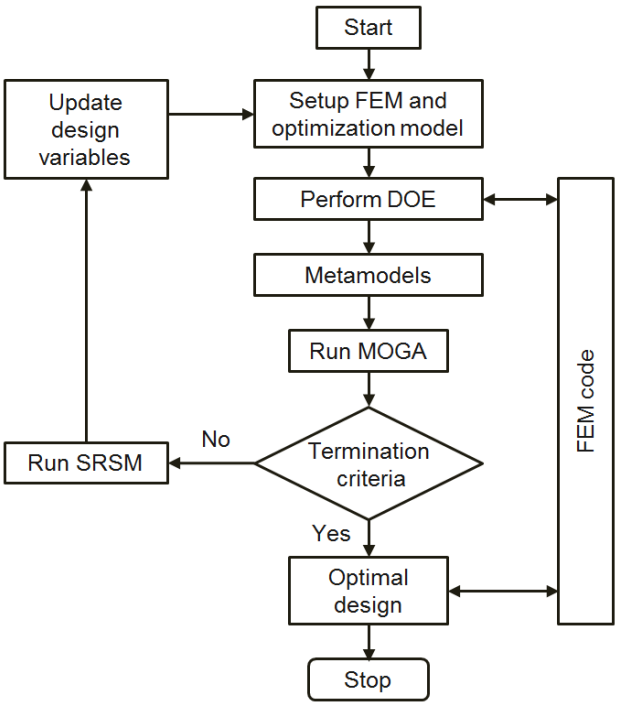

Fig. 8. Set up of optimization

3.4. RESULTS OF THE OPTIMIZATION

The evolution of change in the lengths of the paddle edges is shown as 3D scatter plots in Fig. 9. The design space of the parameters reduces after each iteration. The optimum solution was reported after 8 iterations. The green cubes show the results of simulations with bulge heights within the desired tolerance while the red cubes indicate results with bulge

heights out of the desired tolerance. The failed simulations due to mesh distortion are presented in the white cubes.

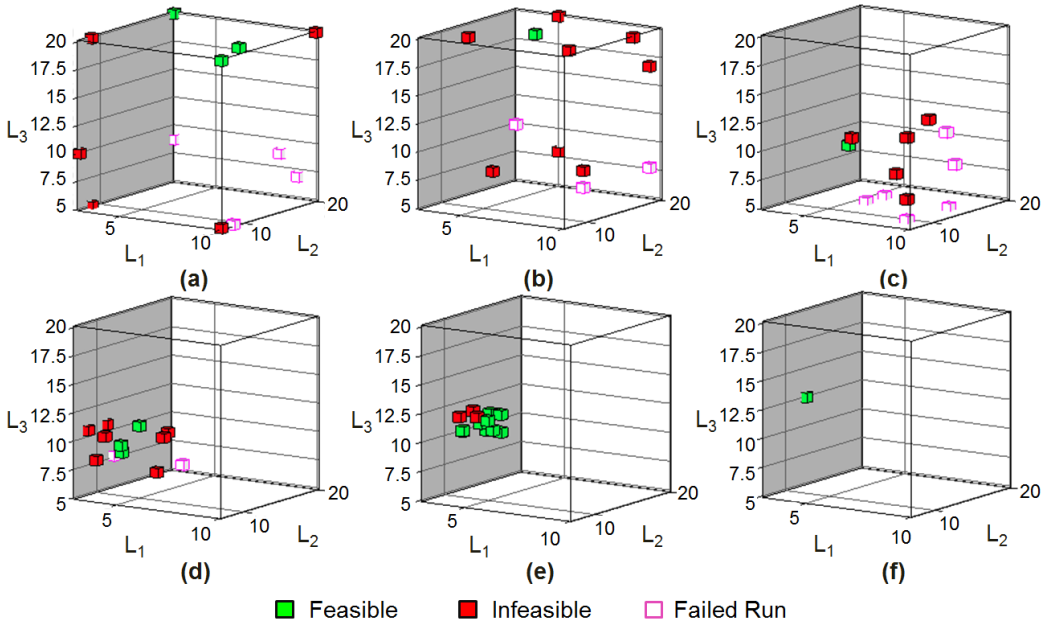

Fig. 9. 3-D scatter plots showing the evolution of the lengths of the forming edges with domain reduction. a) Iteration 1, b) Iteration 2, c) Iteration 3, d) Iteration 5, e) Iteration 7, f) Optimum value

The progress of the paddle shape, the evolution of the principal strains at point B and the bulge heights at the end of selected simulations and iterations of the optimization are shown in Fig. 10. In iteration 1, the paddle has a wide variety of shapes due to a wide range of the design variables. The flanges made by the paddle from the starting variables, the paddles with the maximum and minimum lengths are shown. The paddle on the left represents the starting variables of the optimization. The flange made by this paddle has a high bulge height (1.47 mm) because the large radius at the last egde of the paddle does not pull the blank into the matrix. The principal strains at point B are in the right quadrant of the FLD (biaxial stretching) since the flange is formed by a single edge of the paddle. This strain path is similar to biaxial stretching reported in hole flanging by single stage ISF [15]. The middle paddle forms a flange with a bulge height of 1.08 mm due to the large radius at the last edge of the paddle. The strains at point B are in the left quadrant of FLD (uniaxial tension) because the blank makes contact with multiple edges of the paddle. The paddle on the left side forms a flange with a bulge height of 0.41 mm. The small radius of the last edge of the paddle draws the blank into the matrix. However, because most of the forming of the blank is done by the last forming edge, bending occurs at the clamped end of the blank which leads to a higher bulge height than for the flange obtained by the concave paddle. The blank is in biaxial stretching at point B since most of the forming is done by the small edge.

Iteration 3 shows less variation of the paddle shape due to a reduction of the design space. The paddle on the left forms a flange with the strains at point B undergoing uniaxial tension and the flange has a bulge height of 1.04 mm. The paddle on the right has a bulge height of (0.89 mm) and the strains uniaxial tension.

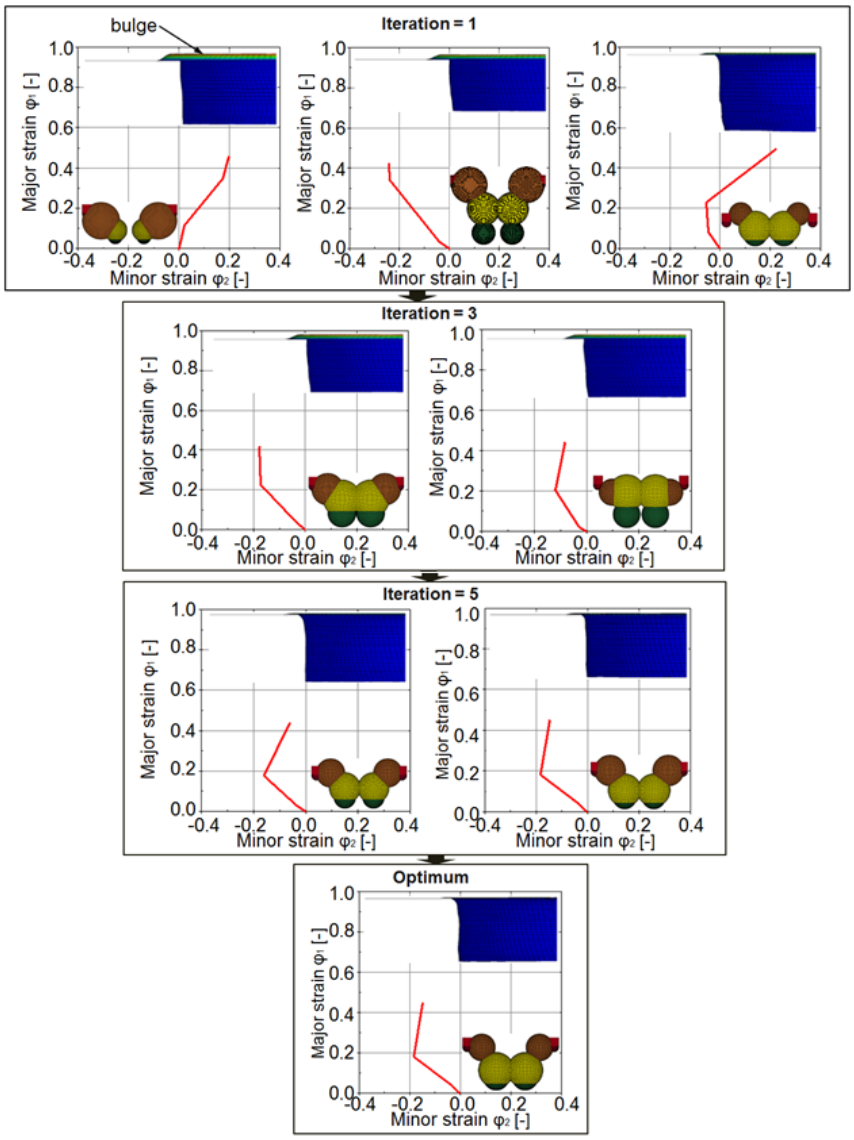

Fig. 10. Evolution of the paddle shape, principal strains, and bulge height during the optimization process

For iteration 5, the paddle shapes are similar due to the reduced design space. The left paddle formed a flange with a bulge height of 0.22 mm while the right paddle formed a flange with a bulge height of 0.21 mm. Both paddles had strains in uniaxial tension.

3D plots of the RS were extracted at the last iteration of the optimization to summarize the correlation between the optimization parameters and the responses (bulge height and principal strains). The last iteration was chosen because the meta model uses knowledge from the previous iterations. Fig. 11 shows that the optimization variables have a linear effect on the maximum bulge height (see node 4 in Fig. 5a). The bulge height increases with increase in R_3 as can be seen in Fig. 11a. This is due to the reduced capacity for a large radius at the edge of the paddle to draw the sheet into the die. The bulge height reduces with increase in R_1 probably due to increased friction as a result of the larger contact area between the paddle and sheet. This draws the sheet into the matrix. R_2 is dependent on R_1, thus their responses are same. R_1 has a lesser effect on the bulge height compared to R_3 because the paddle makes contact with the blank at R_3 after contact at R_1 stops.

L_1 has a negligible correlation with the bulge height as can be seen in Fig. 11b and 11c. The bulge height is high for low values of L_2 and reduces as L_2 increases (Fig. 11c). Low values of L_3 have low bulge heights and the bulge height increases with increase in L_3, see Fig. 11b. L_2 and L_3 have opposite effects on the bulge height as shown in Fig. 11d. Low values of L_3 (final forming step, R_4) stretch the sheet into the matrix which reduces the height of the bulge.

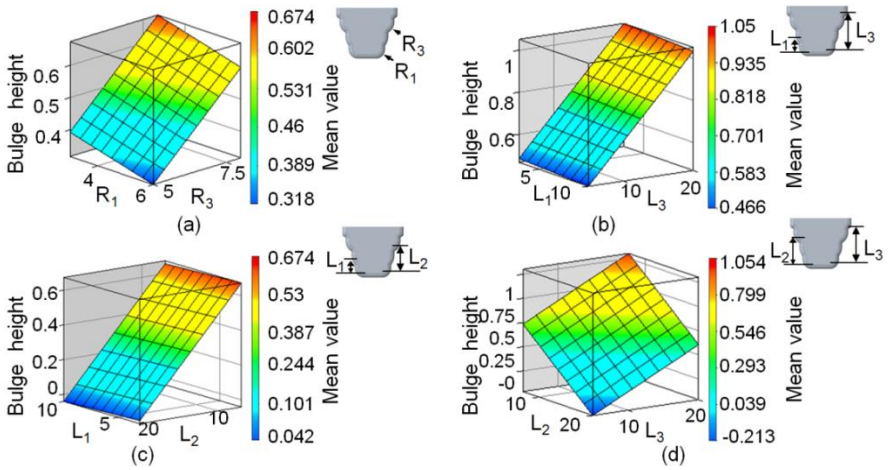

Fig. 11. Response surfaces (RS) showing the effect of the paddle edge radius and length on the height of the bulge at node 4

RS showing the effects of the optimization parameters on the mean value of the strain difference D at point B (element 4, see Fig. 5b) midway along the flange length are presented in Fig. 12. A small value of R_1 coupled with a large R_3 promotes deviation of the principal strains from the desired strain path as shown in Fig. 12a. The small value of R_1 causes biaxial stretching which leads to a large deviation in the strain difference D, R_2 follows a similar trend as R_1. The effect of the change in R_3 on D is less pronounced than the change in R_1.

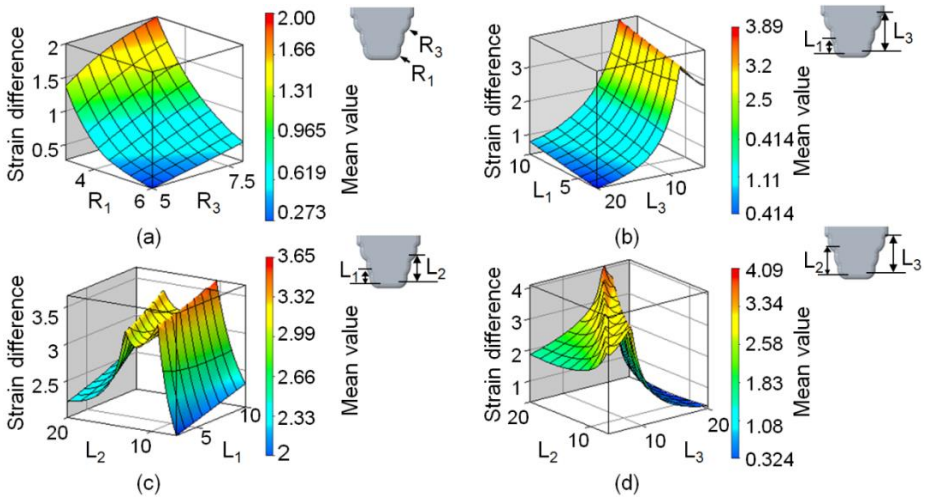

Fig. 12. Response surfaces (RS) showing the effect of the paddle edge radius and length on the strain difference, D of element 4 along the flange length

L_1 has a weak correlation with D as seen in Fig. 12b and 12c. For L_2, the value of D is high towards the middle range of the distribution and low at the boundaries. The magnitude of D for L_2 is largely dependent on its interaction with L_1 and L_3 as demonstrated in Fig. 12c and 12d. Figure 12b shows that L_3 has a strong correlation with D. Small values of L_3 cause high deviation D due to the almost flat paddle shape which causes biaxial stretching. As L_3 increases biaxial stretching reduces because the paddle becomes more convex.

L_3 (length of R_4) has the most significant effect on the process based on the magnitude of the response of the bulge height, see Fig. 11b, 11d, and the difference in strains shown in Fig. 12b and 12d. It is the last step of the paddle to make contact with the flange. The 3rd forming step (L_2 and R_3) are the next most influential parameters on the outcome of the optimization based on the RS in Fig. 11c, 11d, 12c, and 12d. The 2nd and 1st forming edges have a lower influence on the optimization outcome. Table 2 shows the values obtained at the optimum solution. The values of the variables at the optimum solution may change for the same optimization setup due to the randomness of the D-optimal DOE.

Table 2. Table of results

Variable	L_1	L_2	L_3	R_1	R_2	R_3
Optimum value (mm)	3.00	12.44	12.53	5.45	7.45	5.69

The bulge height was 0.18 mm for the flange formed by the optimum paddle shape. This value is within ±0.2 mm tolerance required to apply the process in industry. The principal strains of the flange formed by the optimized paddle shape lie between the strains of the 2 other paddles, as shown in Fig. 13. All the principal strains at point B lie in the left quadrant of the FLD. This indicates a reduced possibility for crack occurrence along the flange length. The tendency for wrinkling was also reduced based on the fewer elements in the wrinkling zone of the FLD (at point C) see Fig. 13c.

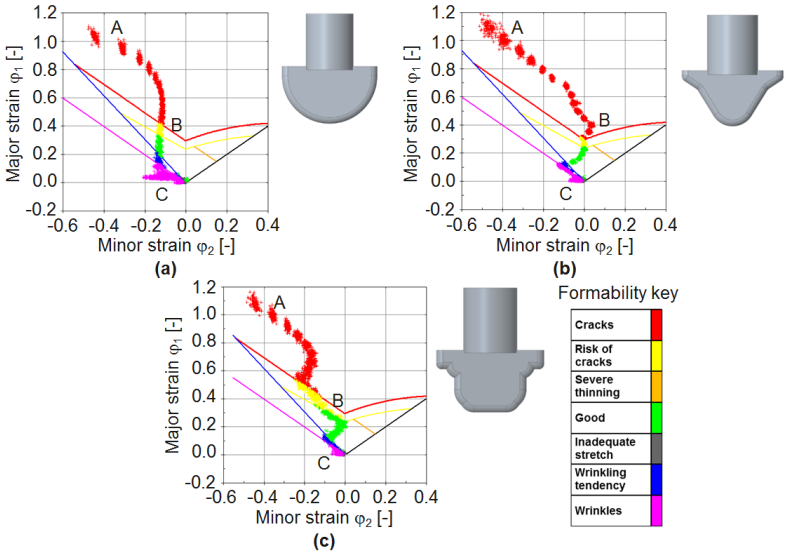

Fig. 13. Principal strains of the flanges: a) Convex paddle shape, b) Concave paddle shape, c) Paddle shape obtained from the optimization

4. CONCLUSIONS AND FUTURE WORK

This study was undertaken to investigate the feasibility of performing hole-flanging operations by paddle forming through the use of FE simulations. The results of the preliminary FE simulations demonstrate the need to optimize the paddle shape in order to prevent cracks along the flange length and bulge formation at the clamped end of the flange. Optimization of the paddle shape was accomplished by using a curve mapping strategy which achieved deformation of elements along the flange length following a pre-defined strain path that prevents biaxial stretching. The principal strains of the middle elements of the flange made by the optimum paddle shape were in the left quadrant (safe zone) of the FLD. The bulge height at the clamped end of the sheet was 0.18 mm for the optimum paddle shape. Thus, both objectives of the optimization were achieved.

The RS from the optimization show that the length of the 4th forming edge (L_3) is the most important parameter in determining the bulge height and the deviation of the principal strains from the FE simulations to the desired strain path (pure shear). The 3rd forming edge has the second highest influence on the process outcome. The 2nd and 1st forming edges have smaller influences.

In future, experiments will be conducted to investigate hole-flanging by paddle forming. The effect of the paddle shape to the hole-flanging process will be studied to validate the FE analyses and the optimization results.

ACKNOWLEDGEMENTS

The authors thank the Europäische Forschungsgesellschaft für Blechverarbeitung e.V., which is a part of AiF-Forschungsvereinigung for the financial support of the project "Roboterbasiertes Kragenziehen" with the no. 20457BG.

REFERENCES

[1] PETEK A., GANTAR G., PEPELNJAK T., KUZMAN K., 2007, *Economical and ecological aspects of single point incremental forming versus deep drawing technology*, Key Engineering Materials, 344, 931–938.
[2] MONTANARI L., CRISTINO V.A., SILVA M.B., MARTINS P.A.F., 2013, *On the relative performance of hole-flanging by incremental sheet forming and conventional press-working*, Proceedings of the IMechE, 228/4, 312–322.
[3] ECHRIF S.B.M., HRAIRI M., 2011, *Research and progress in incremental sheet forming processes*, Materials and Manufacturing Processes, 26/11, 1404–1414.
[4] FILICE L., FRATINI L., MICARI F., 2002, *Analysis of material formability in incremental forming*, CIRP Annals – Manufacturing Technology, 51/1, 199–202.
[5] CUI Z., GAO L., 2010, *Studies on hole-flanging process using multistage incremental forming*, CIRP Journal of Manufacturing Science and Technology, 2/2, 124–128.
[6] BAMBACH M., VOSWINCKEL H., HIRT G., 2014, *A new process design for performing hole-flanging operations by incremental sheet forming*, Procedia Eng., 81, 2305–2310.
[7] ALLWOOD J.M., SHOULER D.R., 2007, *Paddle forming: a novel class of sheet metal forming processes*, CIRP Annals – Manufacturing Technology, 56/1, 257–260.
[8] MARCINIAK Z., DUNCAN J.L., HU S.J., 2002, *Mechanics of sheet metal forming. Second edition*, Oxford, Butterworth-Heinemann.
[9] ALLWOOD J.M., BRAUN D., MUSIC O., 2010, *The effect of partially cut-out blanks on geometric accuracy in incremental sheet forming*, *Journal of Materials Processing Technology*, 210/11, 1501–1510.

[10] BAMBACH M., CANNAMELA M., AZAOUZI M., HIRT G., BATOZ J.L., 2007, *Computer-aided tool path optimization for single point incremental sheet forming*, Advanced Methods in Material Forming, Springer Berlin Heidelberg.
[11] WITOWSKI K, FEUCHT M, STANDER N., 2011, *An effective curve matching metric for parameter identification using partial mapping*, 8th European LS-DYNA, Users Conference Strasbourg, 1–12.
[12] NOVAK N., VESENJAK M., REN Z., 2017, *Computational Simulation and Optimization of Functionally Graded Auxetic Structures Made From Inverted Tetrapods*, Phys. Status Solidi B, 254/12, 160075.
[13] UL HASSAN H., MAQBOOL F., GÜNER A., HARTMAIER A., BEN KHALIFA N., TEKKAYA A.E., 2016 *Spring back prediction and reduction in deep drawing under influence of unloading modulus degradation*, Int. J. Mater. Form., 9, 619–633.
[14] STANDER N., ROUX W., GOEL T., EGGLESTON T., CRAIG K., 2009, *LS-OPT user's manual, a design optimization and probabilistic analysis tool for the engineering analyst*, Livermore Software Technology Corporation (LSTC), Livermore.
[15] MARTÍNEZ-DONAIRE A.J., BORREGO M., MORALES-PALMA D., CENTENO G., VALLELLANO C., 2019, *Analysis of the influence of stress triaxiality on formability of hole-flanging by single-stage SPIF*, International Journal of Mechanical Sciences, 151, 76–84.

APPENDIX

The curve mapping procedure is as follows: the strain path for an element (see Fig. 5b) is divided at points along its length to form segments. A segment (k) is defined by 2 points on the strain path that can be linked by a straight line as shown in Fig A1.

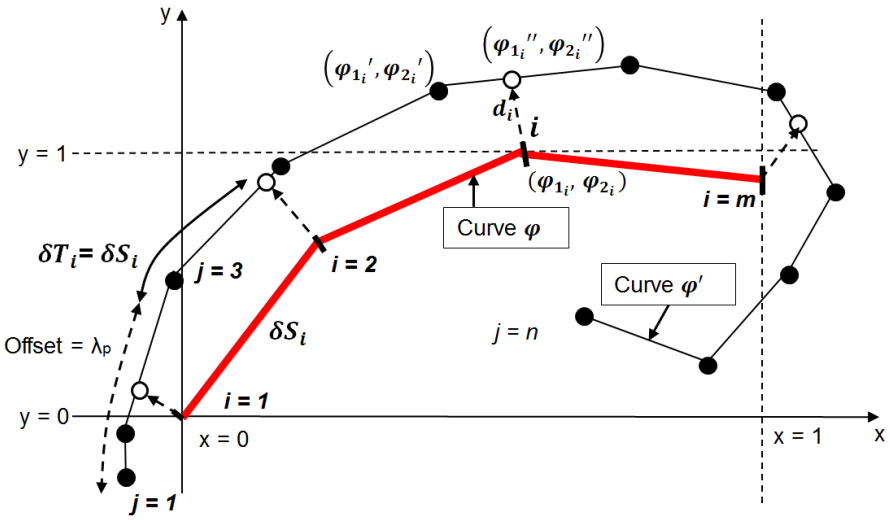

Fig. A1: Partial curve mapping of the principal strains φ (in red) to the predefined strain path φ' with offset. The result is the curve φ''. The solid points represent the original vertices of φ' while the open circles show the mapped points representing φ''. Curves φ and φ' are both normalized to the bounding box of φ in the range [(0,0),(1,1)]

The m point coordinates i of the curve φ (complete curve) are normalised to its smallest bounding box to create curve φ.

$$\varphi_{1i} = \frac{X_i - X_{\min}}{X_{\max} - X_{\min}} \qquad \varphi_{2i} = \frac{Y_i - Y_{\min}}{Y_{\max} - Y_{\min}} \tag{A1}$$

where: $X_{\min} = \min_k X_k$; $X_{max} = \max_k X_k$; $Y_{\min} = \min_k Y_k$; $Y_{\max} = \max_k Y_k$.

Normalize the *n* point coordinates *j* of the computed curve φ' to the smallest bounding box to create curve φ'. See Figure A1.

$$\varphi'_{1j} = \frac{x_j - X_{\min}}{X_{\max} - X_{\min}} \qquad \varphi'_{2j} = \frac{y_i - Y_{\min}}{Y_{\max} - Y_{\min}} \tag{A2}$$

The total length *S*, of the strain path φ is obtained by adding the individual segment lengths δS_i defined by equation A3.

$$\delta S_i = \sqrt{\left(\varphi_{1_i} - \varphi_{1_{i-1}}\right)^2 + \left(\varphi_{2_i} - \varphi_{2_{i-1}}\right)^2}; \qquad i = 2,3,\dots,m \tag{A3}$$

where: φ_1 and φ_2 are the major and minor strains form simulation, *i* is an index for *m* number of segments. Each segment can be scaled by using equation A4.

$$\tilde{s}_i = \delta S_i / S \tag{A4}$$

Similarly the total length *T* of the predefined strain path φ', is obtained by adding segments equation A5.

$$\delta T_i = \sqrt{\left(\varphi'_{1_j} - \varphi'_{1_{j-1}}\right)^2 + \left(\varphi'_{2_j} - \varphi'_{2_{j-1}}\right)^2}; \qquad j = 2,3,\dots,n \tag{A5}$$

where: $\varphi'_1$and φ'_2 are the predefined major and minor strains, *j* is the index for *n* number of segments.

An *offset* is defined as a starting point of a curve section of total length *S* on curve φ'. The offset = λ_p is varied in the range $p = 1$ to *P* so that the strain path φ 'slides' into the predefined strain path φ'. $\lambda \in [0, T - S]$. Assume *P* increments in the interval so that each increment has size.

$$\Delta\lambda = \frac{T - S}{P}; \tag{A6}$$

Set $\lambda_p = \lambda_{p-1} + \Delta\lambda$ to create a new section of φ' create point coordinates by mapping each point of curve φ to curve φ'. A typical curve segment *i* on φ' which corresponds to a segment *i* on φ has a length $\delta T_i = \delta S_i$ (see Fig. 13). This creates a new set of points pairs φ''_1

The area (volume = V_i) between the φ and the new solution φ'' represents a mismatch error. The area is obtained by multiplying the distance d_i between the points to the scale of each segment, see equation A7 and A8.

$$d_i = \sqrt{(\varphi''_1 - \varphi_1)^2 + (\varphi''_2 - \varphi_2)^2} \tag{A7}$$

$$V_i = \frac{d_i + d_{i-1}}{2} \, x \, \tilde{s}_i; \;\; V_i = 0; i = 1,2,3,\dots,m; \tag{A8}$$

where: $\varphi''_1$and φ''_2 are the major and minor strains of the *new* solution. The sum of the areas of the segments D_p represents the difference between the 2 strain paths, equation A9.

$$D_p = \sum_{i=1}^{m} V_i \tag{A9}$$

p is varied until the minimum distance D is found between $\varphi'$and φ''which represents the best match between φ and φ'.

$$D = \min_{p} D_p \tag{A10}$$